The forward-wave and backward-wave behaviors of electromagnetic waves in two-dimensional photonic crystals

Ping Jiang[1*], Huajun Yang[1], Kang Xie[2]

[1]College of Physical Electronics, University of Electronic Science and Technology of China,
 Sichuan Province 610054, China

[2]College of Instrument Science and Opto-electronic Engineering,
 Hefei University of Technology, Hefei 230009, China

*Corresponding author: jiangp@uestc.edu.cn

The negative refractions are discussed in detail to demonstrate two different two-dimensional photonic crystal structures that undergo negative refractions associated with the backward-wave and forward-wave phenomenon, respectively. The presentation of the left-handed property of effective negative index photonic crystal is followed by a discussion of a backward flowing phase and causality. The forward-wave negative refraction occurs in photonic crystals as a result of anisotropy. This paper is based on the theoretical analysis and is illustrated with the results of finite element method simulations.

Keywords: forward-wave behavior, backward-wave behavior, negative refraction, phase velocity, finite element method simulation.

1. Introduction

Currently, negative refraction media are of interest to the scientific community and are engineered materials of functionalities for applications, such as absorbers, filters, couplers, antennas, superlens and superprisms, *etc*. [1, 2]. These media, which are quite different from right-handed (RH) media, are commonly known as metamaterials. Although such a phenomenon was initially met with some skepticism [3], the numerical simulation [4, 5] and experimental evidence [6, 7] have proved the existence of negative refraction. Negative refraction mechanism can be divided into two types, namely local resonance and non-local Bragg scattering. The former does not impose a limit on the sizes of lattice constants, the period of the structure could be much smaller than the working wavelength. Left-handed (LH) material (where Poynting vector $\mathbf{S}$ antiparallels to wave vector $\mathbf{k}$, *i.e.*, $\mathbf{S} \cdot \mathbf{k} < 0$) with simultaneously $\varepsilon < 0$ and $\mu < 0$, which belongs to this mechanism, is approximated to be an isotropic homogeneous medium [8–10].

VESELAGO first pointed out LH negative refraction phenomena in 1968 [11]. Years later, several theoretical and experimental groups have investigated LH materials involving phase velocity antiparallel to group velocity, where each depends upon the wave vector and the energy flow, respectively [12, 13].

Photonic crystals (PhCs) are inhomogeneous materials whose lattice constants are in the order of the wavelength of light and Bragg scattering strength of each scatter is strong. The propagation of light waves inside such lattices will be modified by the photonic bandgap, and negative refraction will be realized in a particular frequency range by the fine design of the band structure. A number of research groups theoretically and experimentally demonstrated negative refraction in the valence band of 2D/3D PhCs operating in the microwave regime [14, 15] and optical regime [16, 17].

However, it appears that a degree of caution is needed because there is more than one mechanism for negative refraction in PhCs. Two common cases are negative refraction with an effective negative index [18, 19] and all-angle negative refraction (AANR) without a negative index [20, 21]. It has been established that some features of effective negative index PhCs are similar to those occurring in LH material, and in which the effective medium method could be probably used [22, 23]. However, there is some disagreement on the mechanism involved in AANR PhCs. Some researchers attribute it to negative photonic effective mass [24], while others provide perhaps much more complicated reasons, such as a tunnelling effect [25].

In this work, we study in detail the issue of negative refraction mechanisms in PhCs. Theoretical analyses and finite element method (FEM) simulations are presented to demonstrate the distinction between effective negative index PhCs and AANR PhCs. Backward-wave negative refraction, or negative phase velocity phenomenon in effective negative index PhCs, will be illustrated in Section 2. Forward-wave negative refraction, or positive phase velocity phenomenon in AANR PhCs will be demonstrated in Section 3.

2. Backward-wave behavior in effective negative index PhC

In this section we consider the backward-wave negative refraction property of 2D hexagonal lattices PhC which can be referred to as effective negative index PhCs in certain frequency range.

2.1. Light refraction in effective index PhC

One of the crucial ideas in a homogenization procedure is that the wavelength of radiation is several times, preferably several orders of magnitude, larger than the underlying polarizable objects (such as atoms and molecules). The equal-frequency contours (EFCs) of any homogeneous isotropic media (or free-space) are straightforwardly obtained from the dispersion relation

$$k^2 = \frac{\omega^2}{c^2}\varepsilon\mu \tag{1}$$

For a propagating solution, *k* must be a real number, which can only be realised as long as relative permittivity ε and relative permeabiltiy μ have the same sign. The EFCs are therefore the circles of radii increasing with frequency. The Poynting vector is simply

$$\mathbf{S} \;=\; \frac{1}{2}\,\mathrm{Re}\!\left[\frac{1}{\omega\mu_0\mu(\omega)}\,\mathbf{k}\right]|\mathbf{E}|^2 \;=\; \frac{1}{2}\,\mathrm{Re}\!\left[\frac{1}{\omega\varepsilon_0\varepsilon(\omega)}\,\mathbf{k}\right]|\mathbf{H}|^2 \qquad (2)$$

where ε_0 and μ_0 are the free-space permittivity and permeability values, $|\mathbf{E}|$ and $|\mathbf{H}|$ are the complex amplitudes of electric and magnetic field in the ($\mathbf{k}$, ω) domain. From Eq. (2), it is clear that for isotropic medium, the phase direction given by the wave vector $\mathbf{k}$ is parallel to the energy flow given by the Poynting vector $\mathbf{S}$ when $\varepsilon > 0$ and $\mu > 0$, or antiparallel to when $\varepsilon < 0$ and $\mu < 0$. Choosing the energy flow direction to be positive, positive $\mathbf{k}$ corresponds to forward wave (or RH propagation where $\mathbf{S}\cdot\mathbf{k} > 0$) whereas negative $\mathbf{k}$ corresponds to backward wave (or LH propagation where $\mathbf{S}\cdot\mathbf{k} < 0$). In the backward-wave media, the sign of the phase velocity, *i.e.*, $\mathbf{v}_p = \omega/\mathbf{k}$, is negative. It can be deduced that either in forward-wave media or backward-wave media, the group velocity $\mathbf{v}_g = \nabla_k\omega(|\mathbf{k}|) = \mathbf{k}|\mathbf{k}|^{-1}[\mathrm{d}\omega(|\mathbf{k}|)/\mathrm{d}|\mathbf{k}|]$, that is often regarded as associated with the velocity at which the energy propagates, is always positive because the energy flow in a transmitting wave must always be away from the source.

In the case of PhCs, the band structure arises as a result of multiple Bragg scattering in a periodic array of dielectric scatterers. In fact, the periodicity of the PhC structure is of the order of the wavelength, and hence homogenization in the classical sense cannot be performed. The dispersion relation indicates that at low frequency, the EFCs in (k_x, k_y) space look like those in isotropic medium: a series of independent circles obeying (in the first approximation) Eq. (1) centered at the symmetry points of the reciprocal lattice (as shown in Fig. 1). For that corresponding frequency range, the PhC can perform as an effective index medium.

In Figure 1 the EFCs map is shown, along with the phase matching condition (*i.e.*, the continuity of the tangential component of the wave vector across an interface). Cir-
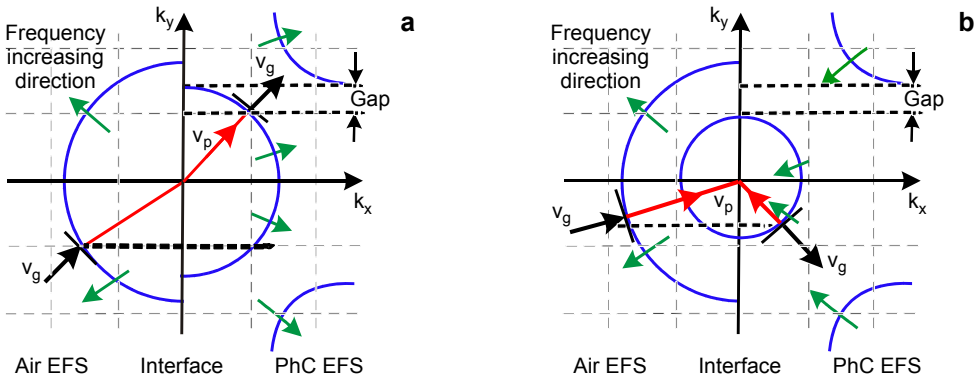

Fig. 1. The schematic illustration of refraction at the interface between isotropic medium and effective index PhCs. Forward-wave positive refraction (**a**), and backward-wave negative refraction (**b**).
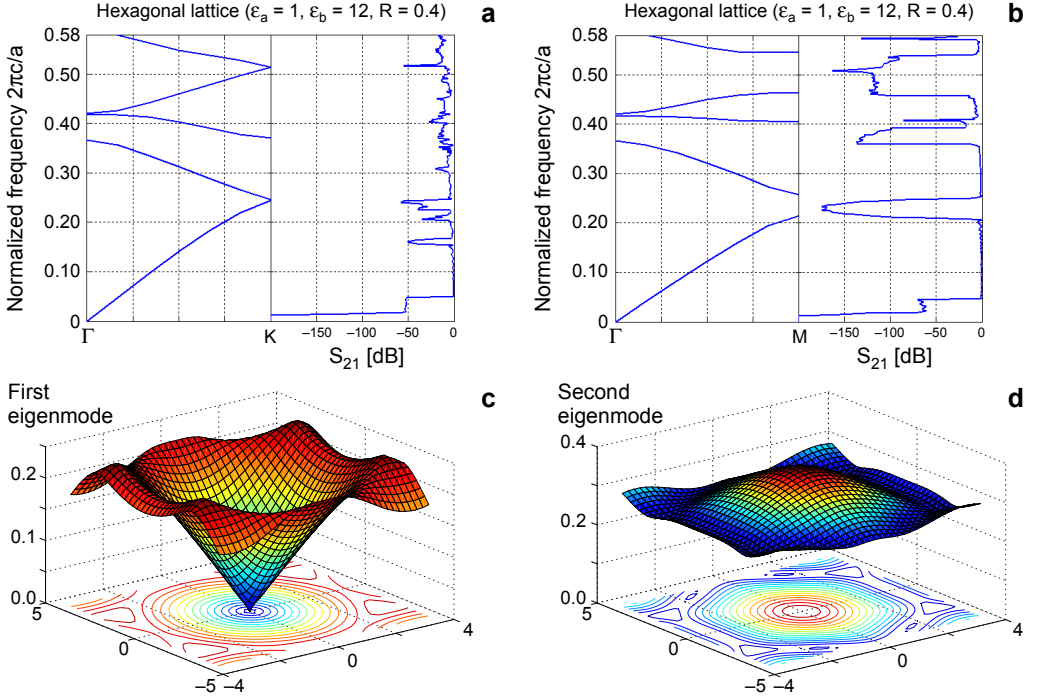
Fig. 2. The TE polarization photonic band curves and eigenmode surfaces of 2D hexagonal lattice PhC. Frequency values are in unit of $2\pi c/a$. Band curves and S_{21} parameters in Γ–M direction (**a**), band curves and S_{21} parameters in Γ–K direction (**b**), and first (**c**) and second (**d**) eigenmode surfaces and their corresponding EFCs.

cles denote EFCs. Dotted arrows denote the increasing direction with frequency. The bold arrows, which are perpendicular to the tangents of the EFCs, show the expected direction of $\mathbf{v}_g$, and hence the energy flow direction. The thin arrows depict the direction of $\mathbf{v}_p$. Figure 1**a** shows the resulting forward-wave positive refraction with the forward flowing phase which is parallel to $\mathbf{v}_g$. As shown in Fig. 1**b**, the $\mathbf{v}_g$ is anti-parallel to $\mathbf{v}_p$ and backward-wave negative refraction is satisfied.

To demonstrate the forward-wave and backward-wave phenomena, we consider a 2D hexagonal lattice PhC formed by air holes in silicon background material with the dielectric constant $\varepsilon_r = 12$. The radius of the air holes is $0.4a$, where a is the lattice constant. The TE polarization (out-plane electronic field) band curves and EFCs are shown in Fig. 2.

It can be seem that the shape of the EFCs is almost circular for the frequency between $\omega = 0.001(2\pi c/a)$ and $\omega = 0.210(2\pi c/a)$ in the first eigenmode, the lower frequency contour is close to the Γ point (the center of circles). And for the frequency between $\omega = 0.300(2\pi c/a)$ and $\omega = 0.360(2\pi c/a)$ in the second eigenmode, the shape of the EFCs is almost circular and higher frequency contour is close to Γ. It has been shown that the relations among effective permittivity, effective permeability, and effective refractive index $n_{\mathrm{eff}} = \varepsilon_{\mathrm{eff}}^{1/2} \mu_{\mathrm{eff}}^{1/2}$ are still valid in this kind of PhC, so-called
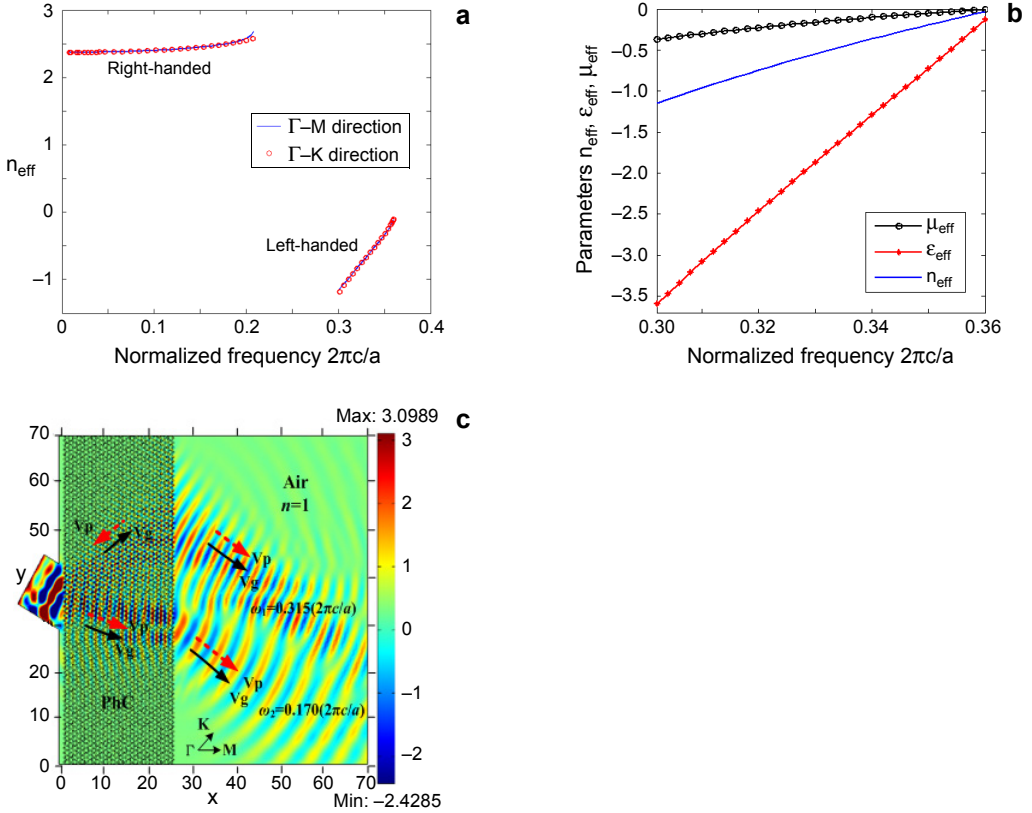
Fig. 3. Effective parameters derived from the averaged eigen-fields using effective medium theory. Effective refractive index n_{eff} of PhC for interface along Γ–M direction (solid line) and along Γ–K direction (circle line) – **a**. Parameters n_{eff}, $\varepsilon_{\mathrm{eff}}$ and μ_{eff} *vs.* normalized frequency in frequency region from $\omega = 0.300(2\pi c/a)$ to $\omega = 0.360(2\pi c/a)$ – **b**. Two light beams with different frequencies incident at a 30 degree angle from air into a PhC interface normal along Γ–M direction; negative refraction at $\omega_1 = 0.315(2\pi c/a)$ corresponding to $n_{\mathrm{eff}} = -1$; positive refraction at $\omega_2 = 0.170(2\pi c/a)$ corresponding to $n_{\mathrm{eff}} = 2.5$ – **c**.

effective index PhCs. These effective parameters can be derived from the averaged ei-gen-fields using the effective medium theory, as shown in Fig. 3**a**. For the frequency between $\omega = 0.001(2\pi c/a)$ and $\omega = 0.210(2\pi c/a)$, the positive n_{eff} is exhibited which is from 2.3 to 2.6, RH positive refraction occurs in this frequency region. For the frequency between $\omega = 0.300(2\pi c/a)$ and $\omega = 0.360(2\pi c/a)$, $\varepsilon_{\mathrm{eff}}$ and μ_{eff} are negative simultaneously (as shown in Fig. 3**b**), thus negative n_{eff} is exhibited. It can be seem that n_{eff} approaches to zero with the frequency of $\omega = 0.360(2\pi c/a)$. Note that when $\varepsilon_{\mathrm{eff}} = -3.1837$ and $\mu_{\mathrm{eff}} = -0.3141$, $n_{\mathrm{eff}} = -1$ is satisfied. LH negative refraction can oc-cur in this frequency region.

One of the principal properties is that of the negative refraction, whereby a ray at $\omega_1 = 0.315(2\pi c/a)$, corresponding to $n_{\mathrm{eff}} = -1$ of PhC, incident from vacuum is re-fracted onto the same side of the normal as the incident beam, as shown in Fig. 3**c**.
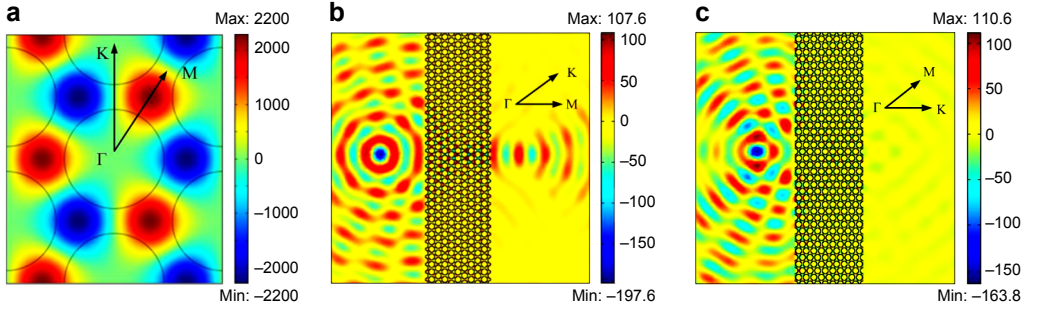
Fig. 4. Investigation into the role the eigenmodes symmetry of the 2D hexagonal PhC lattices plays in the optical response. TE polarized eigenmodes distribution of the PhC, the normalized frequency is $\omega = 0.315(2\pi c/a)$, and black arrows indicate Γ–M and Γ–K directions, respectively – **a**. The FEM simulation results of a point source placed in front of the PhC slab and focus on the other side of the slab, the air–PhC interface is normal to the Γ–M direction – **b**. The case of air–PhC interface normal to the Γ–K direction – **c**.

The $\mathbf{v}_g$, indicated by the solid-line arrow in the figure, is anti-parallel to $\mathbf{v}_p$, indicated by the dotted arrow, and backward-wave negative refraction ensues. On the other hand, for the frequency $\omega_2 = 0.170(2\pi c/a)$, corresponding to $n_{\text{eff}} = 2.5$ of PhC, an incident beam is refracted onto the another side of the normal, and the phase flows in the same direction as the energy, forward-wave positive refraction ensues. It can be seen that the effective index PhC can exhibit amphoteric refractions, and in both cases the Snell law is established.

To verify the effective negative index properties of the PhCs, a simple analysis of a single monochromatic electromagnetic wave incident from air into the PhC interface must be conducted. The symmetry of the eigenmodes of the PhCs plays an important role in their optical response. The eigenmodes which cannot be excited by an external electromagnetic wave are due to the mismatching of their spatial symmetry. Figure 4**a** shows the TE field distributions of the bulk modes at the frequency $\omega = 0.315(2\pi c/a)$, which is in the region of negative refraction. It is clear that the bulk mode has even symmetry for the Bloch wave vectors $\mathbf{k}$ in the Γ–M direction, and odd symmetry in the Γ–K direction. Since the external TE wave from the point source is of even symmetry, only the Bloch waves in PhC with an even symmetry can be excited, that is why a subwavelength imaging can be realized when the PhC slab interface is normal to the Γ–M direction, as shown in Fig. 4**b**. Due to the symmetry mismatch, the coupling coefficient at the interface normal to the Γ–K direction is very small, as shown in Fig. 4**c**.

2.2. Left-handed behavior and causality

The question of causality in the possibility of negative refraction led to a number of doubts and discussions in the scientific community. By causality, energy has to flow in one continuous direction, propagating toward and then away from the interface. With
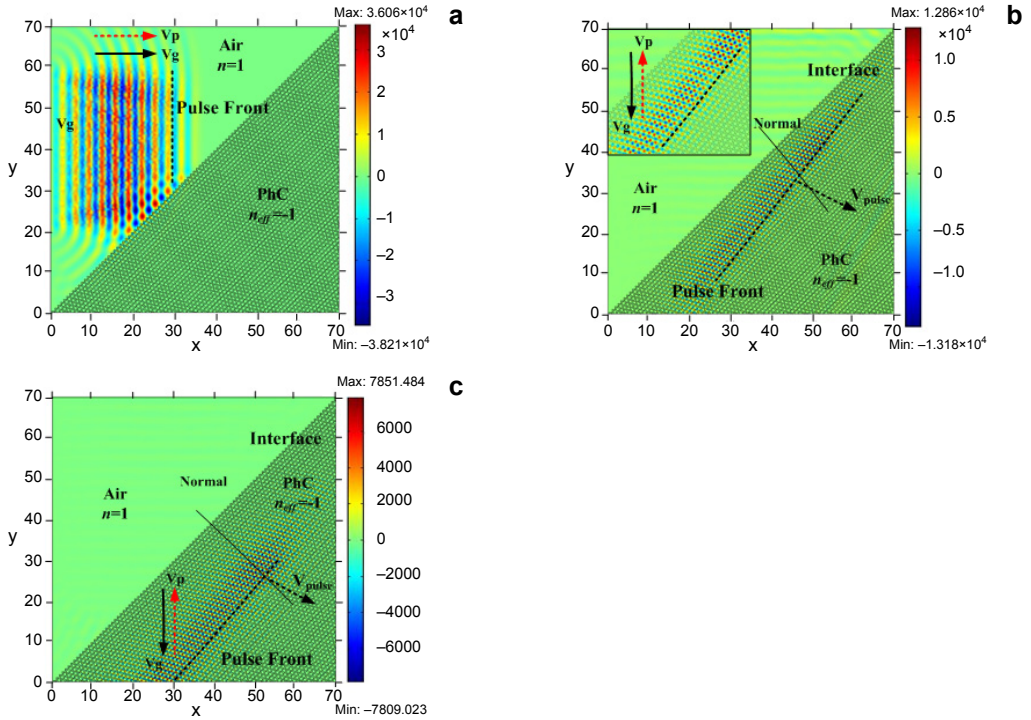
Fig. 5. FEM simulation of a pulse-front crosses an interface between air and an effective index PhC. Negative refraction at $\omega = 0.315(2\pi c/a)$ corresponding to $n_{eff} = -1$ of PhC. The figures are snapshots of how the input pulse is evolving for three sample times: 1.2×10^{-7} s (**a**), 3.9×10^{-7} s (**b**), and 6×10^{-7} s (**c**).

regards to these comments, the refracting property of the pulse front which is associated with the temporal-spatial character of an incident wave will be addressed here. Figure 5 shows for an interface between air ($n = 1$) and PhC with $n_{eff} = -1$ that is inclined at an angle of 45° to the incoming pulse with the frequency of $\omega = 0.315(2\pi c/a)$.

As an initial flat pulse-front, with a velocity of $\mathbf{v}_{pulse}$, meets the interface, it undergoes a positive refraction in PhC (as shown in Fig. 5**b**), which means the temporal character of the pulse is free from the restraints of causality. What is important here, however, is that the $\mathbf{v}_g$ showing the direction of energy flow (to which Snell's law cannot be applied) and $\mathbf{v}_p$ (wave vector $\mathbf{k}$) that are normal to wave fronts (to which Snell's law must be applied) can be used to gain information about the type of refraction taking place. Let's look close at the refraction field profile in the PhC, (as shown in Fig. 5**b**, inset), $\mathbf{v}_p$ labelled with a dotted arrow are flowing anti-parallel to $\mathbf{v}_g$ labelled with a solid-line arrow, and both of them undergo the negative refraction. This is the classic backward-wave behavior similar in the LH medium and it is clear that negative refraction only influences the spatial features in effective negative index PhC. Figure 5**c** reveals that the pulse does not change its shape as it is propagating in PhC, which means this PhC is approximated to be an isotropic homogeneous medium.

3. Forward-wave behaviors in positive phase velocity PhC

It is difficult to make clear distinction between forward and backward wave phenomena. In this part we consider the negative refraction of 2D square lattice PhC which can be referred to as AANR PhCs in certain frequency range.

Figure 6 shows two waves incident at different angles from a positive $\mathbf{v}_p$ medium (*e.g.*, air $n = 1$) onto a typical square lattice PhC. The EFCs of the positive $\mathbf{v}_p$ medium and the PhC both have a positive gradient, *i.e.*, for increasing frequency these contours will sweep out towards increasing $\mathbf{k}$ values, and as a result the $\mathbf{v}_p$ is forward relative to the $\mathbf{v}_g$. For both the positive (as shown in Fig. 6**a**) and negative refraction (as shown in Fig. 6**b**) the phase waves are travelling forward but at an angle to the $\mathbf{v}_g$ direction. It clearly implies that this kind of PhC can be referred to as a positive phase velocity medium, regardless of whether positive or negative refraction is taking place. This is rather different from the properties outlined above for the effective index PhCs that lead directly to antiparallel group and phase velocities. In other words, the anisotropy can cause the Poynting vector and the wave vector to be noncollinear.

To demonstrate the forward-wave negative refraction, we consider a 2D square lattice PhC formed by air holes in silicon background material with dielectric constant $\varepsilon_r = 12$. The radius of the air holes is $0.4a$, where a is the lattice constant. The TM polarized EFCs of the first band are shown in Fig. 7**a**. To realize AANR for superlensing, the required conditions in our model system are that the EFCs are both convex and larger than the EFCs for air (circles with radius ω/c). Incident beams at any incident angle will then experience negative refraction when entering the PhC. The EFM simulation clearly demonstrates that superlensing effect occurs in AANR PhC slab system at the frequency of $0.211(2\pi c/a)$ (as shown in Fig. 7**b**). An infinitely long slab can focus all Fourier components of an image (both the propagation waves and the evanescent waves), and make a perfect image [25].

From the preceding discussion, it is expected that the time-modulation will produce a front that moves in a positive refraction direction and that the space-modulation will
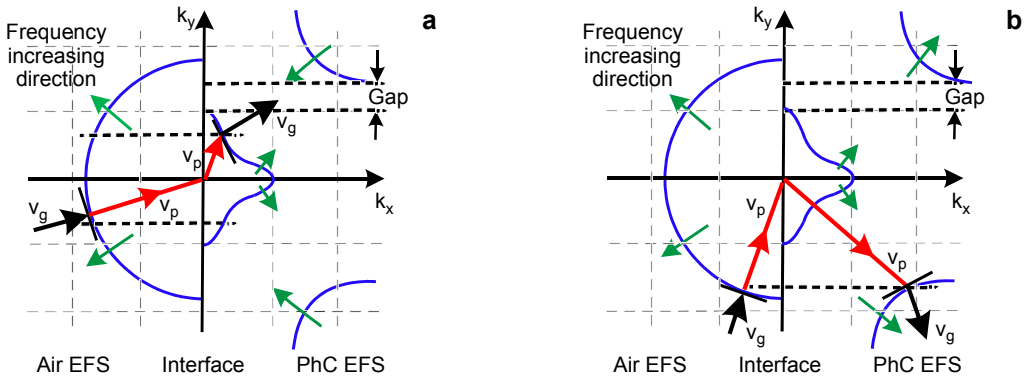

Fig. 6. The schematic illustration of refraction at the interface between isotropic medium and a typical square lattice PhC. Forward-wave positive (**a**) and negative (**b**) refraction.
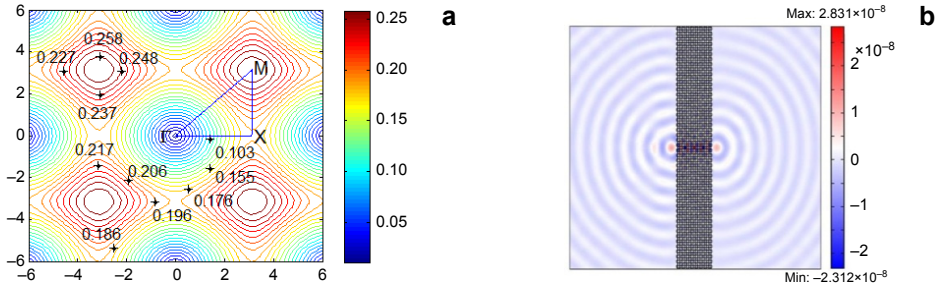
Fig. 7. The TM polarized EFCs of the first band of model AANR PhC (**a**), and superlensing effect at the frequency of $0.211(2\pi c/a)$ which is in the AANR region (**b**).

produce negative refraction of the actual energy flow. Figure 8 shows for an interface between air ($n = 1$) and model AANR PhC that is inclined at an angle of 45° to the incoming pulse with the frequency of $\omega = 0.211(2\pi c/a)$.

It is shown that the pulse-front associated with the time-modulation propagates with a velocity $\mathbf{v}_{pulse}$ and undergoes a positive refraction in PhC (as shown in Fig. 8**b**),
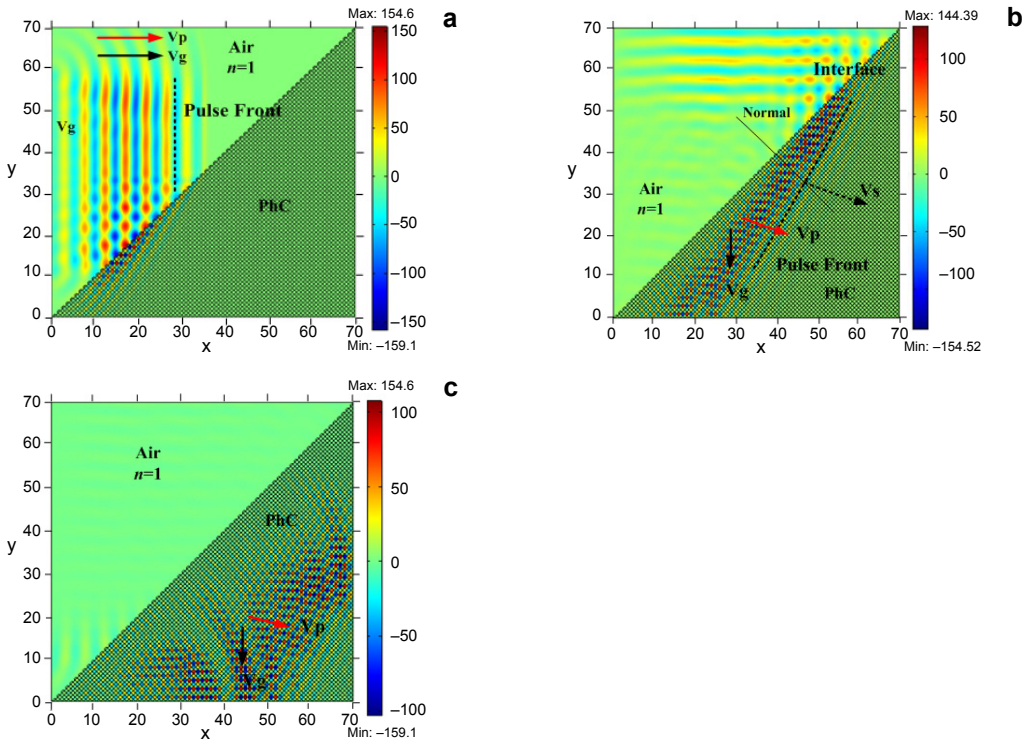

Fig. 8. FEM simulation of a pulse-front at $\omega = 0.211(2\pi c/a)$ crosses an interface between air and the model AANR PhC. The pulse-front and the forward flowing phase undergo a positive refraction in PhC and the group velocity undergoes a negative refraction. The figures are snapshots of how the input pulse is evolving for three sample times: 1.2×10^{-7} s (**a**), 2.4×10^{-7} s (**b**), and 5.1×10^{-7} s (**c**).

and the forward travelling $\mathbf{v}_p$ is with the same direction as the $\mathbf{v}_{pulse}$. The $\mathbf{v}_g$, which undergoes a negative refraction in PhC is noncollinear with the direction of $\mathbf{v}_p$. The pulse becomes distorted as it is propagating in the PhC, as shown in Fig. 9**c**. It is an important evidence that the anisotropy effect is a considerable complication as compared to an isotropy case. This positive $\mathbf{v}_p$ refraction is quite different from the negative $\mathbf{v}_p$ work that is illustrated in Section 2.

4. Conclusions

The concept of forward and backward waves is clearly illustrated in this article in which the direction of the phase front and the energy rays are defined. By using FEM simulation method, it is demonstrated that backward-wave negative refraction occurs in effective index PhCs involving $\mathbf{v}_p$ antiparallel to $\mathbf{v}_g$, and that forward-wave negative refraction occurs in PhCs as a result of anisotropy, in which the Poynting vector and the wave vector are noncollinear. It is wrong to say that negative refraction could be only exhibited in negative $\mathbf{v}_p$ media, and it is also misleading that all negative refraction is connected to backward-wave phenomena. It is demonstrated visually that the time--modulation, which produces a front that undergoes a positive refraction, is free from the restraints of causality, and that the space-modulation will produce negative refraction of the actual energy flow.

References

[1] Taya S.A., El-Agez T.M., Kullab H.M., Abadla M.M., Shabat M.M., *Theoretical study of slab waveguide optical sensor with left-handed material as a core layer*, Optica Applicata **42**(1), 2012, pp. 193–205.

[2] Lei Kang, Qian Zhao, Hongjie Zhao, Ji Zhou, *Magnetically tunable negative permeability metamaterial composed by split ring resonators and ferrite rods*, Optics Express **16**(12), 2008, pp. 8825–8834.

[3] Valanju P.M., Walser R.M., Valanju A.P., *Wave refraction in negative-index media: always positive and very inhomogenous*, Physical Review Letters **88**(18), 2002, article 187401.

[4] Boardman A.D., Egan P., Velasco L., King N., *Control of planar nonlinear guided waves and spatial solitons with a left-handed medium*, Journal of Optics A: Pure and Applied Optics **7**(2), 2005, pp. S57–S67.

[5] Boardman A.D., King N., Velasco L., *Negative refraction in perspective*, Electromagnetics **25**(5), 2005, pp. 365–389.

[6] Pichard H., Richoux O., Groby J.-P., *Experimental demonstrations in audible frequency range of band gap tunability and negative refraction in two-dimensional sonic crystal*, The Journal of the Acoustical Society of America **132**(4), 2012, pp. 2816–2822.

[7] Yangbo Xie, Popa B.-I., Zigoneanu L., Cummer S.A., *Measurement of a broadband negative index with space-coiling acoustic metamaterials*, Physical Review Letters **110**(17), 2013, article 175501.

 [8] PENG DONG, HONG WEI YANG, *Guided modes in slab waveguides with both double-negative and single-negative materials*, Optica Applicata **40**(4) , 2010, pp. 873–882.
 [9] DEMS M., NAKWASKI W., *The modelling of high-contrast photonic crystal slabs using the novel extension of the effective index method*, Optica Applicata **36**(1) , 2006, pp. 51–56.
[10] AMOOGHORBAN E., ASGER MORTENSEN N., WUBS M., *Quantum optical effective-medium theory for loss-compensated metamaterials*, Physical Review Letters **110**(15), 2013, article 153602.
[11] VESELAGO V.G., *The electrodynamics of substances with simultaneously negative values of ε and μ*, Soviet Physics Uspekhi **10**(4) 1968, pp. 509–514.
[12] ZHENG-GAO DONG, SHUANG-YING LEI, MING-XIANG XU, HUI LIU, TAO LI, FU-MING WANG, SHI-NING ZHU, *Negative index of refraction in metallic metamaterial comprising split-ring resonators*, Physical Review E **77**(5), 2008, article 056609.
[13] KANG L., LIPPENS D., *Mie resonance based left-handed metamaterial in the visible frequency range*, Physical Review B **83**(19), 2011, article 195125.
[14] VON RHEIN A., PERGANDE D., GREULICH-WEBER S., WEHRSPOHN R.B., *Experimental verification of apparent negative refraction in low-epsilon material in the microwave regime*, Journal of Applied Physics **101**(8), 2007, article 086103.
[15] KALITEEVSKI M.A., BRAND S., GARVIE-COOK J., ABRAM R.A., CHAMBERLAIN J.M., *Terahertz filter based on refractive properties of metallic photonic crystal*, Optics Express **16**(10), 2008, pp. 7330–7335.
[16] MOUSSA R., FOTEINOPOULOU S., LEI ZHANG, TUTTLE G., GUVEN K., OZBAY E., SOUKOULIS C.M., *Negative refraction and superlens bahavior in a two-demensional photonic crystal*, Physical Review B **71**(8), 2005, article 085106.
[17] LALOUAT L., CLUZEL B., SALOMON L., DUMAS C., SEASSAL C., LOUVION N., CALLARD S., DE FORNEL F., *Real space observation of two-dimensional Bloch wave interferences in a negative index photonic crystal cavity*, Physical Review B **78**(23), 2008, article 235304.
[18] PARIMI P.V., LU W.T., VODO P., SOKOLOFF J., DEROV J.S., SRIDHAR S., *Negative refraction and left--handed electromagnetism in microwave photonic crystals*, Physical Review Letters **92**(12), 2004, article 127401.
[19] DECOOPMAN T., TAYEB G., ENOCH S., MAYSTRE D., GRALAK B., *Photonic crystal lens: from negative refraction and negative index to negative permittivity and permeability*, Physical Review Letters **97**(7), 2006, article 073905.
[20] KEN-MING LIN, GUO G.Y., *Uncoupled modes and all-angle negative refraction in walled honeycomb photonic crystals*, Journal of the Optical Society of America B **25**(12), 2008, pp. C75–C81.
[21] BELHADJ W., GAMRA D., ABDELMALEK F., HAXHA S., BOUCHRIHA H., *Design of two-dimensional photonic crystal structure based in all-angle negative refractive effect for application in focusing systems*, IET Optoelectronics **1**(2), 2007, pp. 91–95.
[22] ZHAOLIN LU, PRATHER D.W., *Calculation of effective permittivity, permeability, and surface impedance of negative-refraction photonic crystals*, Optics Express **15**(13), 2007, pp. 8340–8354.
[23] XIANGDONG ZHANG, *Image resolution depending on slab thickness and object distance in a two-di-mensional photonic-crystal-based superlens*, Physical Review B **70**(19), 2004, article 195110.
[24] CHIYAN LUO, JOHNSON S.G., JOANNOPOULOS J.D., PENDRY J.B., *All-angle negative refraction without negative effective index*, Physical Review B **65**(20), 2002, article 201104(R).
[25] CHIYAN LUO, JOHNSON S.G., JOANNOPOULOS J.D., PENDRY J.B., *Subwavelength imaging in photonic crystals*, Physical Review B **68**(4), 2003, article 045115.